Available online at www.sciencedirect.com
ScienceDirect
Ceramics International 35 (2009) 1513–1520
CERAMICS INTERNATIONAL
www.elsevier.com/locate/ceramint

Tribological behaviors of single and dual sol–gel ceramic films on Ti–6Al–4V

Wenguang Zhang [a,*], Weimin Liu [b], Ying Liu [a], Chengtao Wang [a]

[a] School of Mechanical Engineering, Shanghai Jiao Tong University, Shanghai 200240, China
[b] State Key Laboratory of Solid Lubrication, Lanzhou Institute of Chemical Physics, Chinese Academy of Sciences, Lanzhou 730000, China

Received 14 November 2007; received in revised form 18 June 2008; accepted 8 August 2008
Available online 11 September 2008

Abstract

TiO_2, SiO_2, hydroxyapatite (HA), TiO_2–HA and SiO_2–HA thin films with good biocompatibility were grown on Ti–6Al–4V (coded as TC4) substrate by sol–gel and dip-coating processes from specially formulated sols, followed by annealing at 500 °C. The chemical states of some typical elements in the target films were detected by means of X-ray photoelectron spectroscopy (XPS). High-resolution scanning electron microscopy (SEM) is applied to characterize the surface and cross-sectional morphologies of obtained films. Various phases of the films were characterized by XRD. The tribological properties of thin films sliding against an AISI52100 steel ball were evaluated on a reciprocating friction and wear tester. As a result, the target films were obtained. Compared with the TC4 substrate, all the sol–gel ceramic films are superior in resisting wear. Among all, HA film shows the best resistance while SiO_2 film shows the worst wear resistance both under higher (3 N) and lower load (1 N). TiO_2 shows a good wear resistance under lower load but higher load. Compared with TiO_2, the wear resistance of the dual film TiO_2–HA can be improved under 3 N but deteriorated under 1 N. Compared with SiO_2, the wear resistance of SiO_2–HA is improved both under 3 N and 1 N. Compared with HA, the wear resistances of dual films are deteriorated both under 3 N and 1 N. Under 0.5 N, a very long wear life for TiO_2–HA is also obtained, illustrating that the lower wear resistance of dual films is closely related to the applied load. SEM observation of the morphologies of worn surfaces indicates that the wear of TC4 is characterized by abrasive wear. Differently, abrasion, plastic deformation and micro-crack dominate the wear of ceramic films. The superior friction reduction and wear resistance of HA films are greatly attributed to the slight plastic deformation of the film. Sol–gel is a potential method being applied to implant materials for wear protection according to proper process designs. The single HA film and the dual TiO_2–HA film is suggested for biomedical application from the point of view of wear protection.

Keywords: A. Sol–gel process; C. Friction; Thin film; Ti–6Al–4V; Wear

1. Introduction

Sol–gel method has been receiving increased attention in recent years with respect to varied applications in optical, electrical, and mechanical fields, etc. [1,2]. It also shows great potential and capability on thin film preparation due to its flexibility in composition, morphology and function control on the molecular level. Sol–gel films with various functional properties, such as cell affinity, bone conduction, piezoelectricity, and magnetic performance have been obtained and widely studied [3–5]. Unfortunately, compared with the widely studied functional properties, the mechanical properties of these films are seldom studied [6].

Recently, it is found that the mechanical/tribological properties of the coatings become a dominant factor for the durability and function of the prosthesis under many situations, such as on the prone of the prosthesis or on the surface of artificial tooth where there is fretting or scratch, etc. [7]. Actually, micro-motion exists between the prosthesis and the host widely. Kamachi et al. have made an extensive analysis on failure of stainless steel orthopedic devices, according to their assessment, 74% of the implants failed at the femoral neck region due to fretting fatigue [8]. Under fretting conditions, Ti alloys are not wear resistant enough as a popular used prosthesis material [9]. Abundant researches have been carried out to improve the wear resistance and biocompatibility of Ti alloys [10,11]. However, an ideal method that can improve the wear resistance and biocompatibility

* Corresponding author.
E-mail address: zhwg@sjtu.edu.cn (W. Zhang).

0272-8842/$34.00
doi:10.1016/j.ceramint.2008.08.009

of the prosthesis significantly at the same time is not available currently while the potential applications of sol–gel films for this purpose are still seldom studied [12].

It is well known that intermediate layers can be used to improve the bonding strength as well as other mechanical properties under many conditions [13]. Whether it is also true for sol–gel ceramic films is not well understood yet.

In this study, SiO_2, TiO_2, HA films and TiO_2–HA, SiO_2–HA dual films are prepared by sol–gel and dip-coating method. The tribological performances are investigated and compared. The wear mechanisms are discussed based on SEM observation in detail. The characteristics of dual films are particularly focused on.

2. Experimental

The substrate Ti–6Al–4V (TC4) of 25 cm × 75 cm was cut from a Ti–6Al–4V plate. The composition of Ti–6Al–4V used in this study: 6.70% Al, 4.21% V, 0. 10% Fe, 0.14% O, 0.07% Si, 0.03% C, 0.015% N, 0.003% H, other Ti. The surfaces of TC4 were abraded with 600 # abrasive papers. Prior to the coating process, all the samples were cleaned in an ultrasonic bath with acetone, ethanol and distilled water, respectively for 10 min, then dried in hot air, and finally saved in the desiccator for use.

2.1. Sample preparation

$Ti(OBu)_4$, $(C_2H_5)_4SiO_4$, ethanol, hydrochloric acid, acetylacetone (AcAc), crystal calcium nitrate, methanol and phosphate acid were commercially obtained and used as the raw materials for preparation of the corresponding sols without further purification.

2.1.1. SiO_2 and TiO_2 film

The preparation process of SiO_2 sol from ethanol solution, starting from $(C_2H_5)_4SiO_4$, was as following: The solution was prepared by adding AcAc and water in ethanol, followed by dropping in the required amount of $(C_2H_5)_4SiO_4$ and hydrochloric acid under stirring. The volume fractions of $(C_2H_5)_4SiO_4$, ethanol, hydrochloric acid, acetylacetone, and water in the prepared solution are 7:89.5:0.5:2:1. After stirring the mixed solution at room temperature and relative humidity 50–60% for 0.5 h, a transparent solution was obtained which was then aged for 24 h and served for film preparation. The preparation process of TiO_2 sol is the same as that of SiO_2 except that $(C_2H_5)_4SiO_4$ was replaced by $Ti(OBu)_4$. The corresponding obtained ceramic film coated sample is coded as SiO_2 and TiO_2, respectively.

2.1.2. HA film

The preparation process of HA sol from methanol solution was as following: 9.44 g crystal calcium nitrate was firstly dissolved in 200 ml methanol, followed by dropping into 2.76 g phosphate acid (85 wt%) under vigorous stirring. After stirring the mixed solution at room temperature and relative humidity 50–60% for 0.5 h, a transparent solution was obtained which was then aged for 24 h and served for the film preparation. The corresponding obtained ceramic film coated sample is coded as Ti–HA.

2.1.3. SiO_2–HA and TiO_2–HA film

The used sol for SiO_2–HA and TiO_2–HA films is the same as that of SiO_2, TiO_2 and HA films. Different dipping procedures are applied as following.

SiO_2, TiO_2 and HA films were prepared by dipping the TC4 plate in the corresponding aged solutions at a drawing speed of 38 cm/min. These films were dried at room temperature for 15 min, and then heated to 500 °C at a rate of 10 °C min^{-1} in an atmospheric oven, held there for 60 min annealing, finally cooled in the oven to room temperature. For TiO_2–HA and SiO_2–HA films, the first step is the same as preparing SiO_2 and TiO_2 film, and the second step is to repeat the procedures of HA film preparation on the surface of SiO_2 and TiO_2 films.

2.2. Experimental apparatus and measurements

XPS analysis was conducted on a multi-functional XPS/AES system (Model PHI-5702) by using Mg Kα radiation operating at 250 W and pass energy of 29.35 eV. The binding energy of C1s (284.6 eV) was used as the reference. The depth profiling XPS was performed with Ar^+ ion bombardment. The beam voltage is 2 kV, the beam density 6 nA/cm^2, and the sputter area 1 mm × 1 mm. The worn surfaces of the films were analyzed with SEM (Model JSM-5600LV). The surface and cross-sectional morphologies of coated specimens were observed by scanning electron microscopy and energy dispersive spectroscopy (SEM/EDS, FEI SIRION 200, US) at 20 kV acceleration voltages. The crystal structures of annealed gel specimens under 500 °C were analyzed by X-ray diffractometry (XRD) in a BRUKER-AXS Diffractometer (Bruker company, Germany) with Cu Kα radiation, tube voltage 40 kV and current 40 mA. The angular range for 2θ was from 10 to 70.

The tribological properties of the films were tested on a reciprocating friction and wear tester (Kyowa DF·PM model) at a sliding velocity of 90 mm min^{-1} in ambient conditions (relative humidity: 40–48%). The sliding distance for each pass is 7 mm. The counterpart is a fixed AISI52100 steel ball (diameter 3 mm). The applied normal force is 0.5 N, 1 N and 3 N, respectively. The coefficient of friction and number of sliding passes were recorded automatically. During the whole sliding process, the friction coefficient keeps stable with very little fluctuation for a short period or rises gradually and at last gets to a stable value, which is close to the friction coefficient value of the substrate, then the film is regarded as failure. The corresponding sliding pass numbers are recorded as the wear life of the film. Three replicate tests were carried out for each specimen. The average friction coefficients and wear lives of the three replicate tests were cited in this article. The relative error for the replicate tests was no more than 5%.

3. Results and discussion

3.1. Characterization of the film

It is known that the microstructure and composition of the surfaces are critical for the durability and function of the implants [14]. A rich study has been carried out on the surface

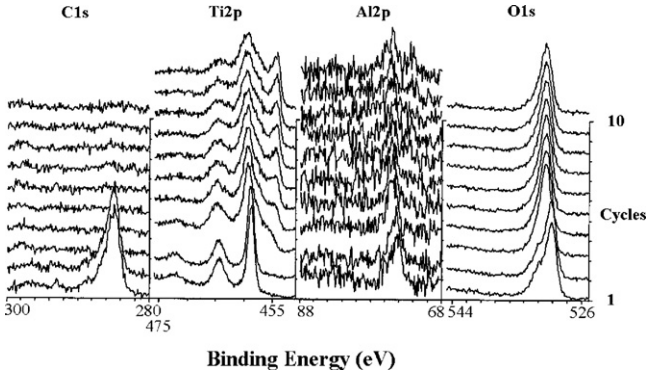

Fig. 1. XPS analysis results of sol–gel TiO_2 film on Ti alloy surface.

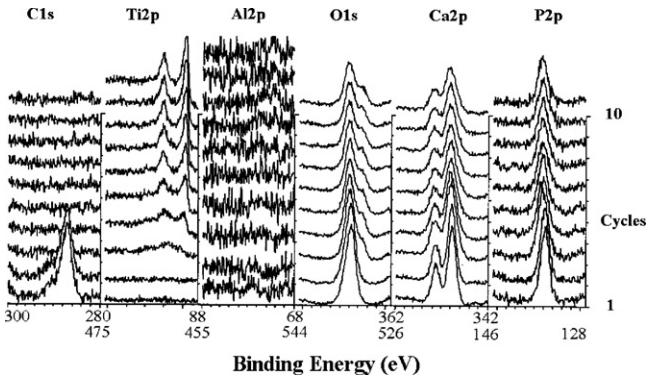

Fig. 2. XPS analysis results of TiO_2–HA film on Ti alloy surface.

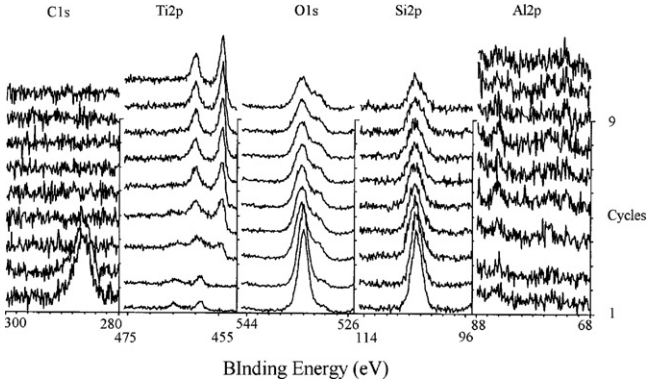

Fig. 3. XPS analysis results of sol–gel SiO_2 film on Ti alloy surface.

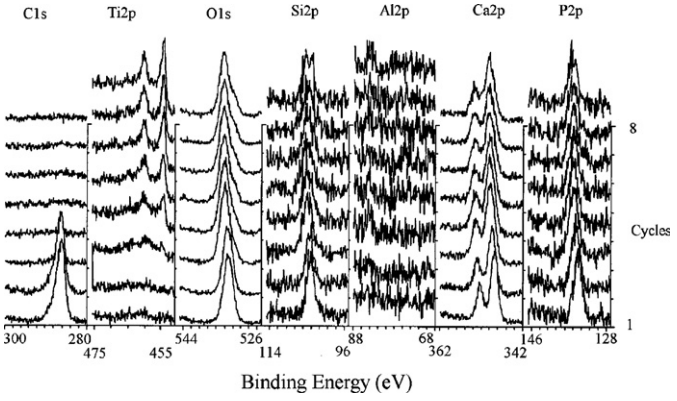

Fig. 4. XPS analysis results of SiO_2–HA film on Ti alloy surface.

structures and compositions of biocompatible films/coatings [15,16].

XPS is applied to detect the chemical states of some typical elements in the target films. Fig. 1 shows the XPS depth profile of TiO_2 film. The binding energy of Ti 458.6 eV [17] indicates that TiO_2 is generated on the very outer surface. Meanwhile, the peak of Al_2O_3 at 74.2 eV [18] also appears. It is worth noting that the Al peak at the very outer surface is stronger than those after sputtering 3 cycles. After 9 sputtering cycles, the peak of Al became strong again. The reason is probably that the Al atom at the nearer surface of the substrate diffused to the very outer surface during

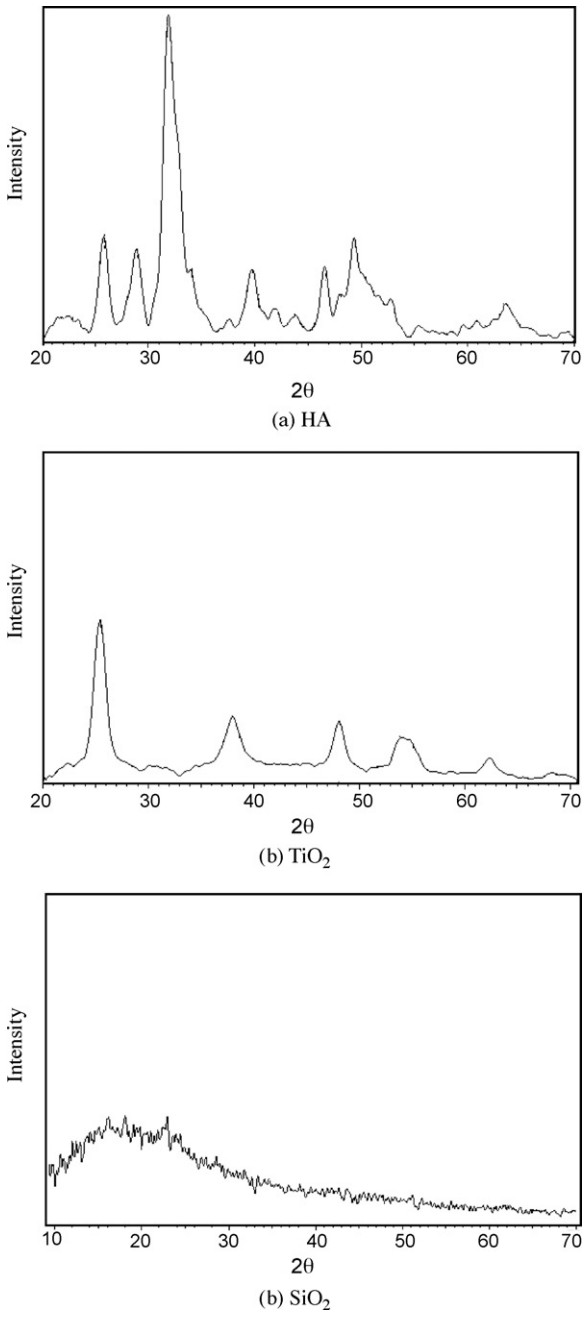

Fig. 5. XRD patterns of HA, TiO_2 and SiO_2 gels annealed under 500 °C (curves a, b and c). (a) HA, (b) TiO_2, and (c) SiO_2.

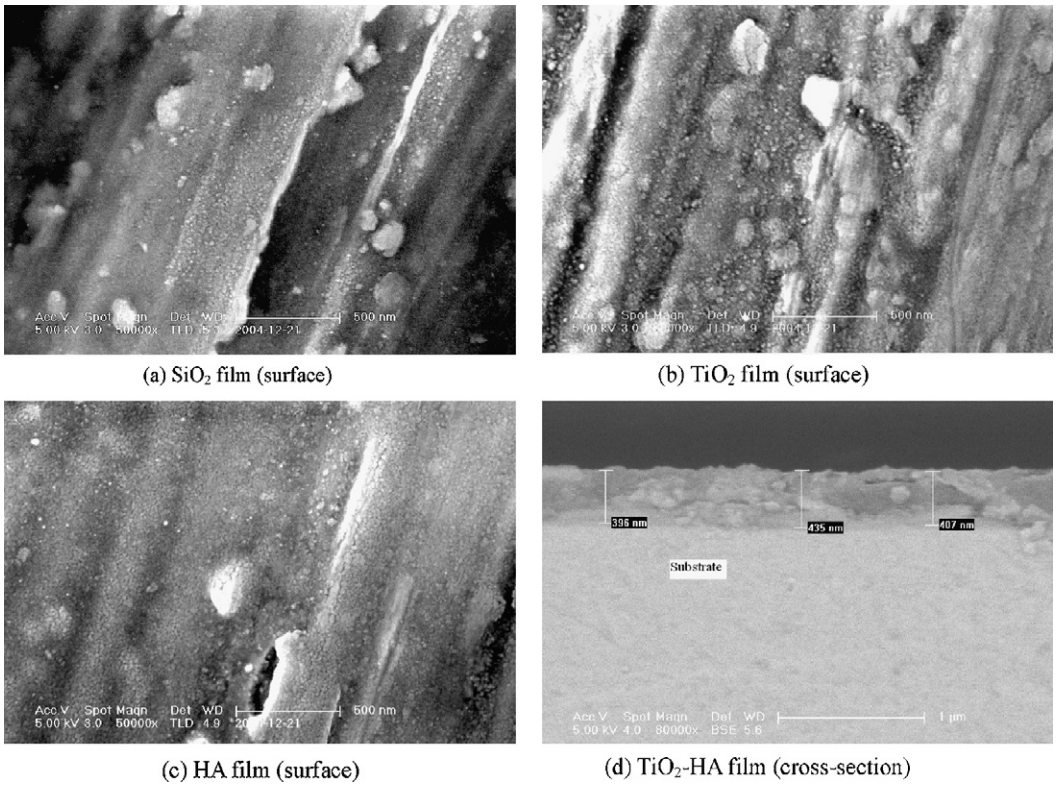

Fig. 6. SEM pictures of the surface morphology and the cross-section of the films. (a) SiO_2 film (surface), (b) TiO_2 film (surface), (c) HA film (surface), and (d) TiO_2–HA film (cross-section).

sintering while the stronger peak of Al atom at deeper place is from the substrate. As shown in Fig. 1, the carbon is only absorbed on the very outer surface.

Fig. 2 shows the XPS depth profile of TiO_2–HA film. The binding energy of Ca_{2p} and P_{2p} is 347.25 eV [19] and 133.0 eV [20], respectively, indicating that the HA film is obtained. During the first several cycles, the peak of Ca and P is very strong while the peaks become weak because the peak of Ti appears and becomes stronger after 3 sputtering cycles. Even so, the regular peak of TiO_2 does not appear. Very possibly, the strength of the Ti oxide is relatively weak because the surface is mainly covered by HA film. The peak of Al is very weak during sputtering because of the coverage of HA film, inferring that multiplayer can reduce the harmful release of aluminum to the body [21]. Interestingly, with sputter going, the peak of O_{1s} becomes asymmetric due to some newly generated oxides, such as TiO, Ti_2O_3, etc. It is deserved to note that the peak of Ca becomes wider during the last several cycles, which may be related to some doping effect of Ti or Ti oxide, or even some new Ca–P compound. In a word, the dual films register very complex composition and the compositions show some characteristics of gradient materials, which is possibly beneficial to the wear resistance and the biocompatibility. Certainly, sol–gel method is efficient and capable to modulate the composition of the surface at a molecular level, which is meaningful to cell affinity. It can be inferred that a promising surface is very possibly to be obtained by sol–gel method based on a proper process design.

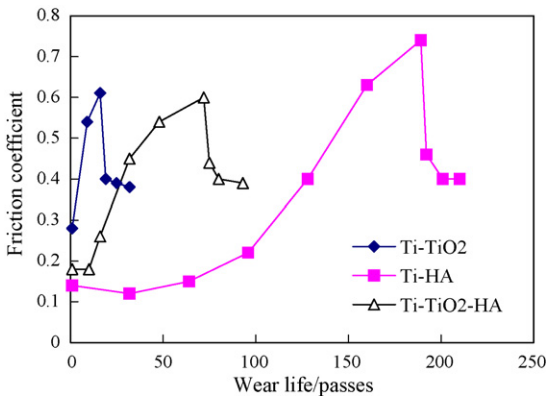

Fig. 7. Tribological results of TiO_2, HA and TiO_2–HA films under 3 N.

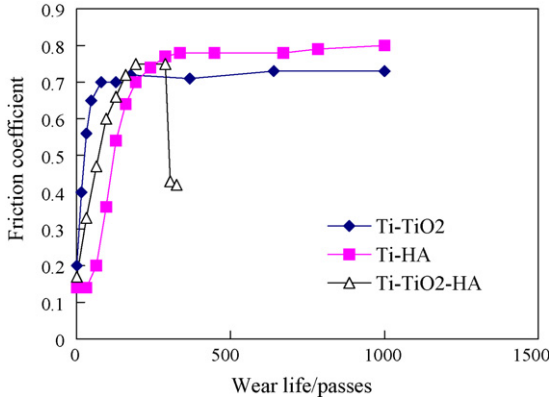

Fig. 8. Tribological results of TiO_2, HA and TiO_2–HA films under 1 N.

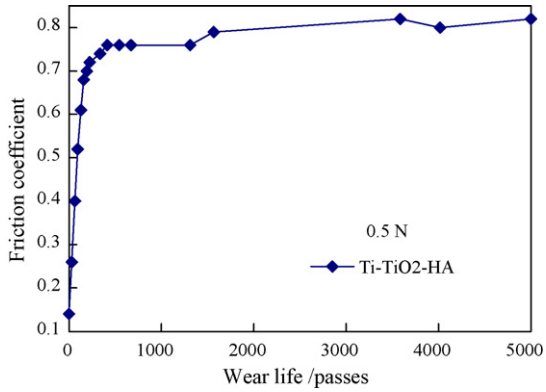

Fig. 9. Tribological results of TiO_2–HA film under 0.5 N.

Fig. 3 shows the XPS depth profile of SiO_2 film. On the very outer surface, several elements, such as Si, Ti, and C exist. After 2 sputtering cycles, C disappears, indicating which is just absorbed on the surface from the contaminated substances but the original reactant. The binding energy of Si_{2p} is 103 eV, which is assigned to SiO_2 [22], indicating that the target film is obtained. At the same time, the peak of Ti also appears, the binding energy of Ti 457.5 eV can be assigned to Ti_2O_3 [23]. And this peak is very weak during the whole sputtering process. With further sputtering, a new peak of Ti 454.1 eV appears which is from the simple Ti of the substrate [24]. Correspondingly, with the sputter going, the intensity of Si becomes weak and the peak of Ti becomes stronger. The peak of Al from the substrate is very weak to determine during the whole sputtering process. After 3 sputtering cycles, the peak of O_{1s} becomes asymmetric at lower binding energy, which is probably caused by some new generated oxides of titanium.

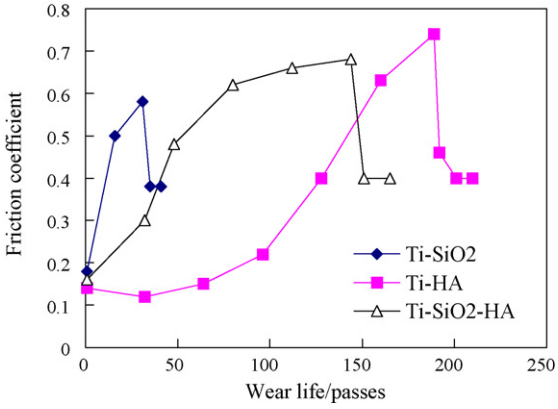

Fig. 10. Tribological results of SiO_2, HA and SiO_2–HA films under 3 N.

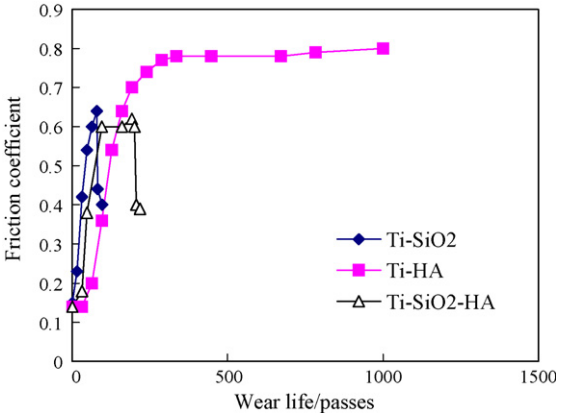

Fig. 11. Tribological results of SiO_2, HA and SiO_2–HA coatings under 1 N.

Table 1
A summary of the sliding passes before failure for different couples under 3 N and 1 N.

Couples	Sliding passes		
	3 N	1 N	0.5 N
TiO_2/steel	32	>1000	
SiO_2/steel	41	97	
HA/steel	210	>2000	
TiO_2–HA/steel	93	325	>5000
SiO_2–HA/steel	165	218	

Fig. 4 shows the XPS depth profile of SiO_2–HA film. The result is similar to that of TiO_2–HA film, i.e. HA film is formed as a main component on the surface. At the same time, with sputter going, Ti_{2p} peak changes. After 4 sputtering cycles, the peak of Ti_{2p} can be ascribed to a Ti oxide and pure Ti, showing some characteristics of gradient materials at the interface.

The crystal structures of HA, TiO_2 and SiO_2 gels annealed under 500 °C were characterized by using XRD, as shown in Fig. 5(a)–(c). Fig. 5(a) shows the XRD patterns of HA gels. There are several major peaks, such as (0 0 2), (2 1 1), (1 1 2) and (3 0 0) at $2\theta = 25.89°$, 31.78°, 32.19°, 32.91°, respectively, which are attributable to a HA structure, indicating that the major phase of the sample annealed under 500 °C is HA. Fig. 5(b) shows the XRD patterns of TiO_2 gels. The major peaks, such as (1 0 1), (0 0 4), (2 0 0) at $2\theta = 25.21°$, 37.83°, 48.02°, respectively, corresponding to the anatase phase of TiO_2, indicate that the TiO_2 film prepared at this temperature is mainly consisted of an anatase phase. The SiO_2 gels annealed at 500 °C are found to be amorphous, as a peak of $2\theta = 22.51°$ appeared (as shown in Fig. 5(c)).

High-resolution SEM is applied to observe the morphologies of the TiO_2, SiO_2, and HA surfaces on a larger scale and the cross-sectional morphology of TiO_2–HA film (see Fig. 6). Grooves are visible on the surfaces, which are very possibly

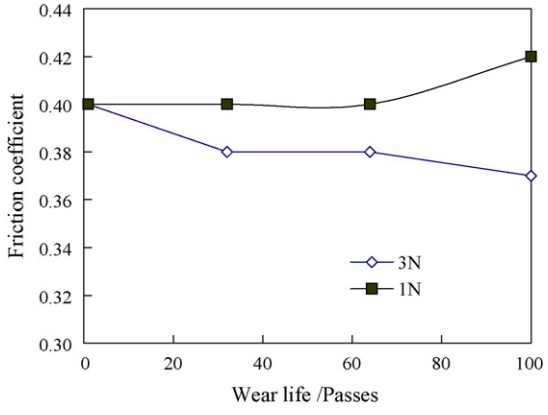

Fig. 12. Tribological results of TC4 at 3N and 1N sliding against AISI52100 steel ball.

caused by the abrasive process during sample preparation. According to the current observation, no very apparent fracture of the films is observed while particles are also observed in the grooves (see Fig. 6(a) and (b)). At the same time, it can be confirmed that the property, such as tightness, of the films are changeable in a larger scale due to the changeable surface morphology (see Fig. 6(a)–(c)). In a word, the films are even in a smaller scale but not on a larger scale. Roughly speaking, the substrate is fully covered by the films composed of nano-particles. Fig. 6(d) shows the cross-sectional image of the TiO_2–HA film. It can be seen that the film is dense and the thickness of the dual film is around 400 nm.

3.2. Friction and wear

The friction and wear behaviors of different TiO_2, HA, and TiO_2–HA films under 3 N are presented in Fig. 7. It can be seen that the TiO_2–HA film is inferior to HA and superior to TiO_2 in wear resistance. It can be inferred that the TiO_2 film between the HA film and the substrate is negative to the longer wear life of the

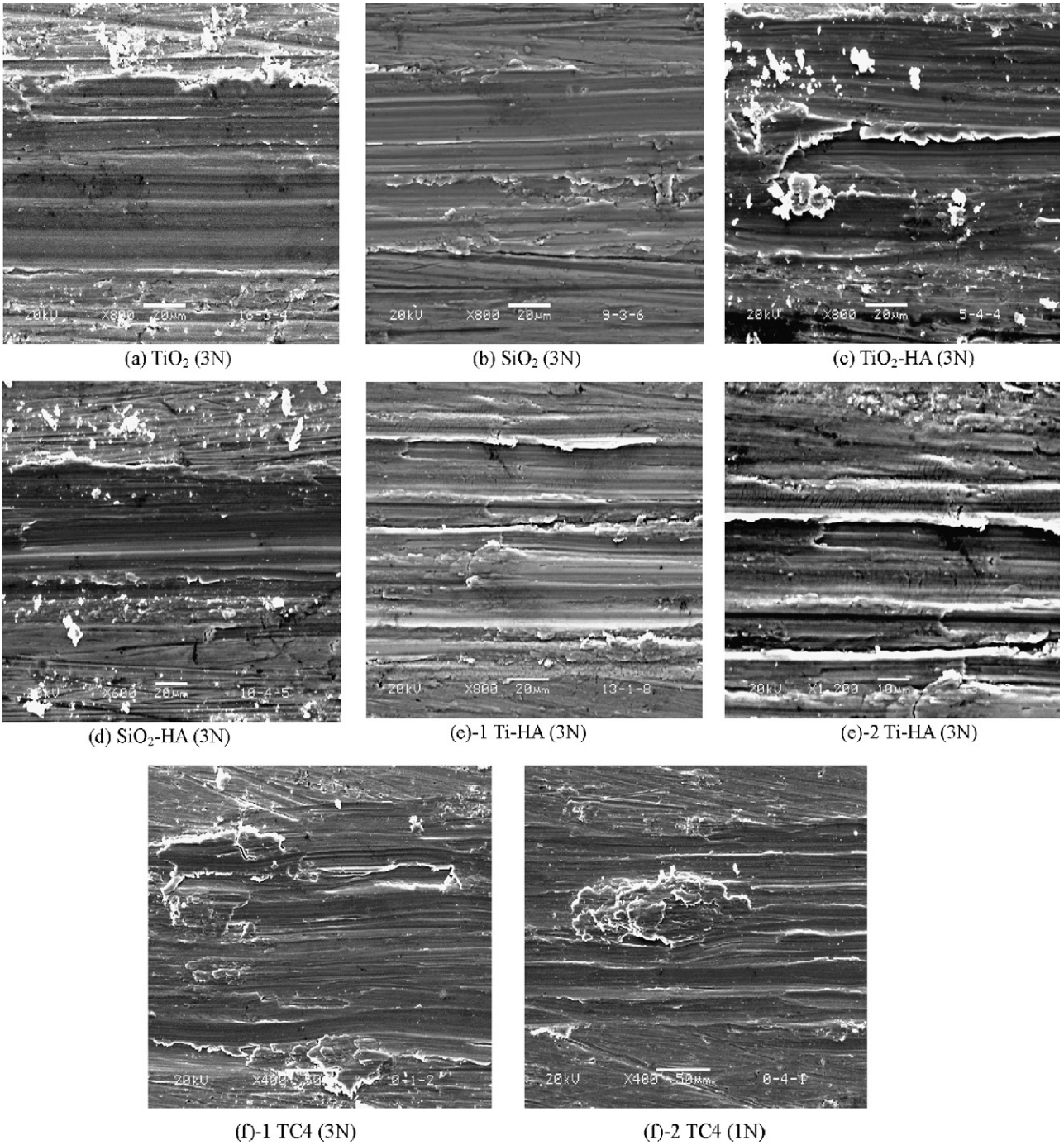

Fig. 13. SEM pictures of worn surfaces of TC4 and sol–gel ceramic films sliding against AISI52100 steel ball. (a) TiO_2 (3 N), (b) SiO_2 (3 N), (c) TiO_2–HA (3 N), (d) SiO_2–HA (3 N), (e) Ti–HA (3 N), (f) TC4 (3 N, 1 N).

dual film due to the following reasons: the interface between HA and TiO_2 film is weak, thus micro-fracture may happen on the interface of HA and TiO_2 easily and generate abrasive particles which in turn increases the failure speed of the film. As the HA film is more wear resistant than TiO_2 the wear life of the TiO_2–HA dual film is still much longer than that of TiO_2. Under 1 N (see Fig. 8), the wear life of the single films of HA and TiO_2 is longer than that of the dual films, indicating that the dual films is more sensitive to the applied load than the single films, which inversely illustrates that the residual stress may exist between the interfaces of the films. Under 0.5 N (see Fig. 9), the wear life of TiO_2–HA is very long, as over 5000 passes, confirming that the wear life is somehow a function of the applied load further. At the same time, a critical value may exist between 1 N and 0.5 N for the dual films. According to the above discussion, the wear life of the dual films is a comprehensive result of the characteristics of interface, the wear resistance of the single films, and the applied loads, etc. And the failure mechanism is supposed to be complicated under different applied loads.

The friction and wear behaviors of different SiO_2, HA, and SiO_2–HA films are presented in Figs. 10 and 11. The order of wear resistance under 3 N and 1 N is as following: HA > SiO_2–HA > SiO_2. This result is similar to that of TiO_2, illustrating that TiO_2 and SiO_2 as intermediate layers are not effective to improve the wear resistance of the dual films compared with HA. This can be explained by the different coefficient of thermal expansion of different materials. As a result, internal stress generated as discussed above. Compare the tribological results of SiO_2–HA with that of TiO_2–HA, under 3 N, TiO_2–HA shows worse wear resistance than SiO_2–HA though the single TiO_2 film shows better wear resistance than the single SiO_2 film, indicating that the bonding between the films and the substrate plays a minor role while the bonding between the films is more important for the dual films. Under a lower load, TiO_2–HA shows a longer wear life, as over 5000 passes, agreeing well with the above-mentioned supposition, i.e., the failure of the dual film is very probably due to its sensitivity to the load caused by the internal stress between the films. If the stress caused by the applied load is not large enough to induce the release of internal stress, the wear life of dual films can be longer. The wear life for different couples is summarized in Table 1. As a comparison, the friction curve of unmodified TC4 is relatively stable with a value about 0.4 (see Fig. 12).

In order to gain more insights into the friction and wear mechanisms, the worn surfaces of TC4 and sol–gel ceramic films sliding against an AISI52100 steel ball have been observed by SEM. As shown in Fig. 13, the worn surfaces of TiO_2 and SiO_2 films are relatively smooth (see Fig. 13(a) and (b)). Differently, abundant fine wear particles are observed on the surface of TiO_2–HA and SiO_2–HA (see Fig. 13(c) and (d)), indicating that sever fracture happened during wear processes. It can be inferred that the wear mechanism of the dual films is partly different from the single ones considering the different mechanical states, such as interlayer stress, internal stress, friction-induced stresses, etc. It seems that fracture easily happened on dual films, agreeing well with the above tribological results. Differently, on the surface of HA, apparent deformation happened, which accounts for the longest wear life of HA (Fig. 13(e)). It is further inferred that SiO_2 and TiO_2 as intermediate layers may inhibit the deformation of HA and cause sever fracture, which in turn deteriorates the wear resistance of the dual films. It can be concluded that the wear mechanism of HA is characteristic of deformation, micro-fracture and abrasive wear while the wear mechanism of the dual films is dominated by fracture and abrasive wear. As a comparison, apparent abrasive wear and plastic deformation happened on the surface of TC4 both under higher (3 N) and lower load (1 N) after 100 passes, indicating that TC4 is too weak to resist wear (Fig. 13(f)).

4. Conclusions

All the single and dual ceramic films have been successfully prepared by sol–gel and dip-coating method on the surface of TC4, which are all effective in resisting wear compared with pure TC4. For the single films, under 3 N, TiO_2 and SiO_2 show similar wear resistance while HA shows the best wear resistance. Under 1 N, HA and TiO_2 register very superior wear resistance and SiO_2 is still very inferior to resist wear. Compared with TiO_2, the wear resistance of the dual film TiO_2–HA is improved under 3 N but deteriorated under 1 N. Compared with SiO_2, the wear resistance of SiO_2–HA is improved both under 3 N and 1 N. Compared with HA, the wear resistances of dual films are deteriorated both under 3 N and 1 N. Under 0.5 N, a longer wear life for TiO_2–HA is also obtained, illustrating that the lower wear resistance of dual films is closely related to the applied load. It can be inferred that the interface of dual films is inferior under higher stress and recycled load, accounting for the shorter wear lives. The wear mechanism of HA is characteristic of deformation, micro-fracture and abrasive wear while the wear mechanism of the dual films is dominated by fracture and abrasive wear.

It can be concluded that all the films register superior wear resistance under a lower load (0.5 N) while under higher load as 1 N, HA and TiO_2 films are recommended, under 3 N, HA, TiO_2–HA and SiO_2–HA films are proposed for wear protection of the titanium alloy prosthesis.

Acknowledgements

The authors gratefully acknowledge the financial support from the National Natural Science Foundation of China (Grant No. 30300078) as well as Medical and Engineering (Science) Cross Research Fund of Shanghai Jiao Tong University (Grant No. YG2007MS17). They are also grateful to Engineer Bo Wang, Jiazheng Zhao and the engineers from Instrumental Analysis Center of Shanghai Jiao Tong University for their assistance in XPS, XRD, and SEM analyses.

References

[1] B.L. Wang, L.L. Hu, Optical and surface properties of hybrid TiO_2/ormosil planar waveguide prepared by the sol–gel process, Ceram. Int. 32 (2006) 7–12.

[2] V. Liedtke, I. Huertas Olivares, M. Langer, Y.F. Haruvy, Manufacturing and performance testing of sol/gel based oxidation protection systems for re-usable space vehicles, J. Eur. Ceram. Soc. 27 (2007) 1493–1502.

[3] A. Balamurugan, G. Balossier, S. Kannan, J. Michel, J. Faure, S. Rajeswari, Electrochemical and structural characterisation of zirconia reinforced hydroxyapatite bioceramic sol–gel coatings on surgical grade 316L SS for biomedical applications, Ceram. Int. 33 (2007) 605–614.
[4] Z.H. Wang, W.G. Zhu, C. Chao, C.L. Zhao, X.F. Chen, Characterization of composite piezoelectric thick film for MEMS application, Surf. Coat. Technol. 198 (2005) 384–388.
[5] P. Delobelle, G.S. Wang, E. Fribourg-Blanc, D. Remiens, Mechanical properties measured by nano-indentation of Pb(Zr, Ti)O_3 sol–gel films deposited on Pt and $LaNiO_3$ electrodes, Surf. Coat. Technol. 201 (2006) 3155–3162.
[6] T. Hübert, S. Svoboda, B. Oerte, Wear resistant alumina coatings produced by a sol–gel process, Surf. Coat. Technol. 201 (2006) 487–491.
[7] A. Shenhar, I. Gotman, S. Radin, P. Ducheyne, Microstructure and fretting behavior of hard TiN-based coatings on surgical titanium alloys, Ceram. Int. 26 (2000) 709–713.
[8] M.U. Kamachi, T.M. Sridhar, N. Eliaz, R. Baladev, Failures of stainless steel orthopedic devices—causes and remedies, Corros. Rev. 21 (2003) 231–267.
[9] A. Vadiraj, M. Kamaraj, Effect of surface treatments on fretting fatigue damage of biomedical titanium alloys, Tribol. Int. 40 (2007) 82–88.
[10] S. Radin, P. Ducheyne, Controlled release of vancomycin from thin sol–gel films on titanium alloy fracture plate material, Biomaterials 28 (2007) 1721–1729.
[11] J. Stallard, S. Poulat, D.G. Teer, The study of the adhesion of a TiN coating on steel and titanium alloy substrates using a multi-mode scratch tester, Tribol. Int. 39 (2006) 159–166.
[12] N. Mirhosseini, P.L. Crouse, L. Li, D. Garrod, Combined laser/sol–gel synthesis of calcium silicate coating on Ti–6Al–4V substrates for improved cell integration, Appl. Surf. Sci. 253 (2007) 7998–8002.
[13] Y.C. Yang, B.Y. Chou, Bonding strength investigation of plasma-sprayed HA coatings on alumina substrate with porcelain intermediate layer, Mater. Chem. Phys. 104 (2007) 312–319.
[14] D.A. Puleo, A. Nanci, Understanding and controlling the bone–implant interface, Biomaterials 20 (1999) 2311–2321.
[15] S. Kaciulis, G. Mattogno, L. Pandolfi, M. Cavalli, G. Gnappi, A. Montenero, XPS study of apatite-based coatings prepared by sol–gel technique, Appl. Surf. Sci. 151 (1999) 1–5.
[16] J.G.C. Wolke, J.P.C.M. van der Waerden, H.G. Schaeken, J.A. Jansen, In vivo dissolution behavior of various RF magnetron-sputtered Ca-P coatings on roughened titanium implants, Biomaterials 24 (2003) 2623–2629.
[17] D. Simon, C. Perrin, J. Bardolle, J. Microsc. Spectrosc. Electron. 1 (1976) 175.
[18] B.R. Strohmeier, D.M. Hercules, J. Phys. Chem. 88 (1984) 4922.
[19] W.J. Landis, J.R. Martin, J. Vac. Sci. Technol. A2 (1984) 1108.
[20] H. Takadama, H.M. Kim, T. Kokubo, T. Nakamura, XPS study of the process of apatite formation on bioactive Ti–Al–4V alloy in simulated body fluid, Sci. Technol. Adv. Mater. 2 (2001) 389–396.
[21] D. Zaffe, C. Bertoldi, U. Consolo, Accumulation of aluminium in lamellar bone after implantation of titanium plates, Ti–6Al–4V screws, hydroxyapatite granules, Biomaterials 25 (2004) 3837–3844.
[22] M.L. Miller, R.W. Linton, Anal. Chem. 57 (1985) 2314.
[23] F. Werfel, O. Brummer, Phys. Scripta 28 (1983) 92.
[24] S. Badrinarayanan, S. Sinha, A.B. Mandale, J. Electron Spectrosc. Relat. Phenom. 49 (1989) 303.